



**HAL**  
open science

## **Trehalose-Based Nucleolipids as Nanocarriers for Autophagy Modulation: An In Vitro Study**

Anthony Cunha, Alexandra Gaubert, Julien Verget, Marie-Laure Thiolat,  
Philippe Barthélémy, Laurent Latxague, Benjamin Dehay

► **To cite this version:**

Anthony Cunha, Alexandra Gaubert, Julien Verget, Marie-Laure Thiolat, Philippe Barthélémy, et al.. Trehalose-Based Nucleolipids as Nanocarriers for Autophagy Modulation: An In Vitro Study. *Pharmaceutics*, 2022, 14 (4), pp.857. 10.3390/pharmaceutics14040857 . inserm-03642513

**HAL Id: inserm-03642513**

**<https://inserm.hal.science/inserm-03642513>**

Submitted on 15 Apr 2022

**HAL** is a multi-disciplinary open access archive for the deposit and dissemination of scientific research documents, whether they are published or not. The documents may come from teaching and research institutions in France or abroad, or from public or private research centers.

L'archive ouverte pluridisciplinaire **HAL**, est destinée au dépôt et à la diffusion de documents scientifiques de niveau recherche, publiés ou non, émanant des établissements d'enseignement et de recherche français ou étrangers, des laboratoires publics ou privés.

## Article

# Trehalose-Based Nucleolipids as Nanocarriers for Autophagy Modulation: An In Vitro Study

Anthony Cunha<sup>1,2</sup>, Alexandra Gaubert<sup>1</sup>, Julien Verget<sup>1</sup>, Marie-Laure Thiolat<sup>2</sup>, Philippe Barthélémy<sup>1</sup>, Laurent Latxague<sup>1,†,‡</sup> and Benjamin Dehay<sup>2,\*,‡</sup>

- <sup>1</sup> Univ. Bordeaux, INSERM U1212, CNRS UMR 5320, ARNA, ARN: Régulations Naturelle et Artificielle, ChemBioPharm, 146 rue Léo Saignat, F-33076 Bordeaux, France; antcunha@u-bordeaux.fr (A.C.); alexandra.gaubert@u-bordeaux.fr (A.G.); julien.verget@u-bordeaux.fr (J.V.); philippe.barthelemy@inserm.fr (P.B.); laurent.latxague@u-bordeaux.fr (L.L.)
- <sup>2</sup> Univ. Bordeaux, CNRS, IMN, UMR 5293, F-33000 Bordeaux, France; marie-laure.thiolat@u-bordeaux.fr
- \* Correspondence: benjamin.dehay@u-bordeaux.fr
- † Deceased 13 December 2021.
- ‡ These authors contributed equally to this work.

**Abstract:** The Autophagy Lysosomal Pathway is one of the most important mechanisms for removing dysfunctional cellular components. Increasing evidence suggests that alterations in this pathway play a pathogenic role in Parkinson's disease, making it a point of particular vulnerability. Numerous studies have proposed nanotechnologies as a promising approach for delivering active substances within the central nervous system to treat and diagnose neurodegenerative diseases. In this context, the aim was to propose the development of a new pharmaceutical technology for the treatment of neurodegenerative diseases. We designed a trehalose-based nanosystem by combining both a small natural autophagy enhancer molecule named trehalose and an amphiphilic nucleolipid conjugate. To improve nucleolipid protection and cellular uptake, these conjugates were formulated by rapid mixing in either solid lipid nanoparticles ( $\text{Ø} = 120.4 \pm 1.4$  nm) or incorporated into poly(lactic-co-glycolic acid) nanoparticles ( $\text{Ø} = 167.2 \pm 2.4$  nm). In vitro biological assays demonstrated a safe and an efficient cellular uptake associated with autophagy induction. Overall, these nucleolipid-based formulations represent a promising new pharmaceutical tool to deliver trehalose and restore the autophagy impaired function.

**Keywords:** nucleolipids; nanoparticles; PLGA; trehalose; autophagy



**Citation:** Cunha, A.; Gaubert, A.; Verget, J.; Thiolat, M.-L.; Barthélémy, P.; Latxague, L.; Dehay, B. Trehalose-Based Nucleolipids as Nanocarriers for Autophagy Modulation: An In Vitro Study. *Pharmaceutics* **2022**, *14*, 857. <https://doi.org/10.3390/pharmaceutics14040857>

Academic Editors: Massimo Conese, Waldemar Debinski and Giuseppe Trapani

Received: 21 March 2022

Accepted: 8 April 2022

Published: 13 April 2022

**Publisher's Note:** MDPI stays neutral with regard to jurisdictional claims in published maps and institutional affiliations.



**Copyright:** © 2022 by the authors. Licensee MDPI, Basel, Switzerland. This article is an open access article distributed under the terms and conditions of the Creative Commons Attribution (CC BY) license (<https://creativecommons.org/licenses/by/4.0/>).

## 1. Introduction

Due to their prevalence, high societal costs, and the absence of disease-modifying or neuroprotective therapeutic strategies, one of the major challenges today lies in discovering new therapies for neurodegenerative diseases (NDD). Parkinson's disease (PD) is the second most common NDD after Alzheimer's disease [1]. PD is characterized by a selective neuronal vulnerability, including degeneration in specific brain regions hosting dopaminergic neurons and deposits of misfolded  $\alpha$ -synuclein-rich protein aggregates [2]. Among the pathological mechanisms involved in the pathogenesis of PD, alteration of the lysosomal function of dopaminergic neurons is of increasing interest in PD research. Lysosomal impairment is now described as a major contributor to the pathogenesis of this disease [3]. Indeed, lysosomes are organelles responsible for the clearance, through autophagy, of long-lived proteins, such as  $\alpha$ -synuclein, which tend to aggregate due to their misfolding. In PD,  $\alpha$ -synuclein aggregation interferes with cellular homeostasis and impairs cellular degradation systems, leading to neuronal death. Thus, restoring lysosomal function represents one of the attractive pathological targets for developing new therapeutic approaches. Trehalose belongs to the therapeutic arsenal against lysosomal failure. Trehalose is a non-reducing disaccharide widely used in the food industry [4], which has

recently shown unique properties, particularly in preventing neurodegeneration. Trehalose can act as a potent protein stabilizer, preserving the structural integrity of proteins and inducing autophagy to improve the clearance of toxic proteins [5–7]. Trehalose treatment reduced the level of toxic protein aggregates, thereby improving behavioural symptoms and survival in animal models of neurodegenerative diseases, including Alzheimer's [8], Parkinson's [9,10], and Huntington's diseases [11]. However, this small molecule is widely distributed upon administration and needs to be specifically delivered to the damaged brain neurons.

One approach to overcoming this limitation relies on the use of nanotechnologies [12,13] such as poly(lactic-co-glycolic acid) nanoparticles (PLGA NPs) [14,15] and solid lipid nanoparticles (SLNs) based on nucleolipids (NLs) [16,17]. First, PLGA NPs present many advantages for their use in the biomedical field due to their biocompatibility, improved drug solubility, efficient targeting, better cellular internalization, . . . [18]. Previous studies showed that empty PLGA NPs restored lysosome acidification failures, particularly in experimental models of PD [19–22]. Second, NL-based SLNs also represent good candidates [23] due to their bio-inspired nature, biocompatibility, biological activities (antimicrobial properties, antifungal, antiviral, antitumor, . . . ), and their remarkable self-assembly capacity [24,25]. Indeed, these amphiphilic molecules can form supramolecular objects such as SLNs, micelles, or liposomes, which can be used to carry active substances, such as deoxyribonucleic acid (DNA), antisense oligonucleotides or small interfering ribonucleic acid (siRNA) directly into cells [26]. Moreover, thanks to molecular recognition, nucleosides can pass cellular membranes through specific transporters, while their lipidization allows their absorption by passive diffusion [27,28]. In addition, we have recently demonstrated that the latter was a good strategy for facilitating passage across the blood brain barrier (BBB), as in the case of uridine with a lipidic diketal (C15), used as a neurotracer, which successfully crossed the BBB [29]. Despite the many advantages of nanotechnology for the delivery of active substances, only a few studies have focused on the delivery of trehalose using nanovectors for the treatment of neurodegenerative diseases, including PD [30–32].

In this study, we report the synthesis of trehalose-NLs (hereafter called **GNLs** for glyco-nucleolipids) embedded in PLGA NPs and SLNs as original nanosystems. We demonstrated *in vitro* that the combination of trehalose and NL did not induce any cellular toxicity, while it improved the uptake and internalization of **GNLs** into neuronal cells associated with the trehalose-induced autophagy effect. The encouraging results described herein suggest that **GNL**-based nanovectors may be efficient pharmaceutical nanocarriers for trehalose delivery.

## 2. Materials and Methods

### 2.1. Procedure for Glyconucleolipids Synthesis

All reactions were performed under an argon atmosphere. Unless otherwise stated, yields were determined on chromatographically and spectroscopically (nuclear magnetic resonance ( $^1\text{H-NMR}$ )) homogeneous materials. All reagent-grade chemicals were purchased from commercial suppliers and used as received, unless otherwise stated.  $^1\text{H-NMR}$  and  $^{13}\text{C-NMR}$  spectra were acquired at 293 K (unless otherwise indicated) on a Bruker Avance 300 ( $^1\text{H}$ : 300 MHz,  $^{13}\text{C}$ : 75.46 MHz) spectrometer with residual  $\text{CHCl}_3$  used as internal reference (7.26 ppm). The chemical shifts ( $\delta$ ) and coupling constants ( $J$ ) were indicated in ppm and Hz, respectively. The following abbreviations were applied to explain the multiplicities: s = singlet, d = doublet, t = triplet, q = quartet, m = multiplet, b = broad. Fourier Transform InfraRed (FT-IR) spectra were acquired on a Perkin-Elmer spectrometer Spectrum two (UATR two). A Waters Micromass ZQ instrument equipped with an electrospray source (positive and/or negative mode) was used for the electrospray ionization high-resolution mass spectrometry (ESI HRMS) analyses. Matrix-assisted laser desorption ionization—time of flight (MALDI TOF) mass spectrometric analyses, using 3,4-dihydroxybenzoic acid as the matrix, were performed on a PerSeptive

Biosystems Voyager-De Pro MALDI mass spectrometer in the Linear mode. Analytical thin-layer chromatography was performed using silica gel 60 F254 pre-coated plates (Merck Millipore, Saint Quentin Fallavier, France) with a revelation by UV light, potassium permanganate or sulfuric acid solutions. Silica gel (0.043–0.063 mm) was used for flash chromatography.

### 2.2. Synthesis of Compound 1: 5'-Azido-5'-deoxythymidine

Triphenylphosphine (1.2 equiv., 2.6 g, 9.91 mmol), sodium azide (5 equiv., 2.68 g, 41.3 mmol) and carbon tetrabromide (1.2 equiv., 3.29 g, 9.91 mmol) were sequentially added to a solution of thymidine (1 equiv., 2 g, 8.26 mmol), in anhydrous dimethylformamide (DMF) (40 mL) and under argon. The mixture was stirred for 24 h at room temperature until completion of the reaction. The reaction was then quenched by the addition of an aq.  $\text{NaHCO}_3$  solution (50 mL) and the resulting mixture diluted with water (30 mL). Three extractions with dichloromethane (DCM;  $3 \times 30$  mL) were applied to the aqueous phase, before drying the combined organic phases over  $\text{Na}_2\text{SO}_4$  and concentrating to dryness under vacuum. A purification of the resulting crude by flash chromatography on a silica gel (DCM/MeOH, gradient 99:1 to 95:5) was required to obtain the expected compound **1** as a white powder (1.63 g, 74%). NMR data were consistent with the literature [33].  $R_f$ : 0.37 (DCM/MeOH, 95:5).  $^1\text{H NMR}$  (300 MHz, MeOD)  $\delta$  (ppm): 1.90 (d,  $J = 0.9$  Hz, 3H,  $\text{CH}_3$  thymidine), 2.25–2.33 (m, 2H,  $\text{H}_{2'}$ ), 3.56 (dd,  $J = 3.9$  Hz, 13.2 Hz, 1H,  $\text{H}_{5a'}$ ), 3.66 (dd,  $J = 5.1$  Hz, 13.5 Hz, 1H,  $\text{H}_{5b'}$ ), 3.96 (q,  $J = 3.9$  Hz, 9 Hz, 2H,  $\text{H}_{4'}$ ), 4.32–4.37 (m, 1H,  $\text{H}_{3'}$ ), 6.27 (t,  $J = 6.9$  Hz, 1H,  $\text{H}_{1'}$ ), 7.54 (s, 1H,  $\text{H}_6$ ).

### 2.3. Synthesis of Compound 2: 3-(5'-Azido-5'-deoxythymidin-3-yl) Methyl Propanoate

DBU (diazabicycloundecene) (1.55 equiv., 433  $\mu\text{L}$ , 2.90 mmol) and methyl acrylate (1.55 equiv., 261  $\mu\text{L}$ , 2.90 mmol) were sequentially added to a solution of **1** (1 equiv., 0.500 g, 1.87 mmol) in anhydrous DMF (2 mL) and under argon. The mixture was stirred overnight at 60 °C until the completion of the reaction and followed by concentration to dryness under vacuum. The resulting crude was purified by flash chromatography on a silica gel (DCM/MeOH, gradient 98:2 to 96:4) to obtain the expected compound **2** as a colorless oil (0.436 g, 66%).  $R_f$ : 0.43 (DCM/MeOH, 95:5).  $^1\text{H NMR}$  (300 MHz,  $\text{CDCl}_3$ )  $\delta$  (ppm): 1.89 (d,  $J = 0.9$  Hz, 3H,  $\text{CH}_3$  thymidine), 2.09–2.23 (m, 1H,  $\text{H}_{2'a}$ ), 2.28–2.41 (m, 1H,  $\text{H}_{2'b}$ ), 2.59 (t,  $J = 7.5$  Hz, 2H,  $\text{H}_B$  linker), 3.55 (dd,  $J = 3.6$  Hz, 13.2 Hz, 1H,  $\text{H}_{5a'}$ ), 3.68 (dd,  $J = 3.0$  Hz, 12.9 Hz, 1H,  $\text{H}_{5b'}$ ), 3.62 (s, 3H,  $\text{H}_C$  linker), 4.01 (q,  $J = 3.6$  Hz, 1H,  $\text{H}_{4'}$ ), 4.18 (t,  $J = 7.8$  Hz, 2H,  $\text{H}_A$  linker), 4.33–4.43 (m, 1H,  $\text{H}_{3'}$ ), 6.26 (t,  $J = 6.9$  Hz, 1H,  $\text{H}_{1'}$ ), 7.34 (s, 1H,  $\text{H}_6$ ).  $^{13}\text{C NMR}$  (75.46 MHz,  $\text{CDCl}_3$ )  $\delta$  (ppm): 13.3 ( $\text{CH}_3$  thymidine), 32.1 ( $\text{CH}_2$ -B linker), 37.2 ( $\text{CH}_2$ -A linker), 40.2 ( $\text{C}_{2'}$ ), 51.9 ( $\text{CH}_3$ -C linker), 52.2 ( $\text{C}_{5'}$ ), 71.4 ( $\text{C}_{3'}$ ), 84.5 ( $\text{C}_{4'}$ ), 85.5 ( $\text{C}_{1'}$ ), 110.4 ( $\text{C}_5$ ), 133.9 ( $\text{C}_6$ ), 150.6 (C=O thymidine), 163.2 (C=O thymidine), 171.9 (C=O linker).

### 2.4. Synthesis of Compound 3: 3-[3'-O-(tert-butyldimethylsilyl)-5'-azido-5'-deoxythymidin-3-yl] Methyl Propanoate

TBDMSCl (*tert*-Butyldimethylsilyl chloride) (1.2 equiv., 0.220 g, 1.46 mmol) and imidazole (1.2 equiv., 0.099 g, 1.46 mmol) were sequentially added to a solution of **2** (1 equiv., 0.430 mg, 1.22 mmol) in anhydrous DMF (2.6 mL) and under argon. The mixture was stirred overnight at room temperature until the completion of the reaction. DCM was added and the precipitate formed was filtered. The mixture was then diluted with toluene (100 mL), and DMF was co-evaporated under vacuum to obtain a yellow oil. The resulting crude was purified by flash chromatography on a silica gel (petroleum ether/EtOAc, 70:30) to obtain the expected compound **3** as a colorless oil (0.491 g, 86%).  $R_f$ : 0.63 (petroleum ether/EtOAc, 70:30).  $^1\text{H NMR}$  (300 MHz,  $\text{CDCl}_3$ )  $\delta$  (ppm): -0.05 (s, 6H,  $\text{CH}_3$ -Si), 0.75 (s, 9H,  $^t\text{Bu}$ ), 1.80 (s, 3H,  $\text{CH}_3$  thymidine), 1.97–2.24 (m, 2H,  $\text{H}_{2'}$ ), 2.49 (t,  $J = 7.5$  Hz, 2H,  $\text{H}_B$  linker), 3.38 (dd,  $J = 3.9$  Hz, 13.5 Hz, 1H,  $\text{H}_{5a'}$ ), 3.48–3.59 (m, 4H,  $\text{H}_C$  linker et  $\text{H}_{5b'}$ ), 3.78–3.85 (m, 1H,  $\text{H}_{4'}$ ), 4.09 (t,  $J = 7.8$  Hz, 2H,  $\text{H}_A$  linker), 4.19–4.27 (m, 1H,  $\text{H}_{3'}$ ), 6.13 (t,  $J = 6.6$  Hz, 1H,  $\text{H}_{1'}$ ), 7.20 (s, 1H,  $\text{H}_6$ ).  $^{13}\text{C NMR}$  (75.46 MHz,  $\text{CDCl}_3$ )  $\delta$  (ppm): -5.17 ( $\text{CH}_3$ -Si), -4.9 ( $\text{CH}_3$ -

Si), 13.0 (CH<sub>3</sub> thymidine), 17.6 (C<sub>q</sub> tBu), 25.4 (CH<sub>3</sub> <sup>t</sup>Bu), 31.8 (CH<sub>2</sub>-B linker), 36.8 (CH<sub>2</sub>-A linker), 40.4 (C<sub>2'</sub>), 51.4 (CH<sub>3</sub>-C linker), 51.5 (C<sub>5'</sub>), 71.5 (C<sub>3'</sub>), 84.6 (C<sub>4'</sub>), 85.3 (C<sub>1'</sub>), 110.0 (C<sub>5</sub>), 133.4 (C<sub>6</sub>), 150.3 (C=O thymidine), 162.7 (C=O thymidine), 171.3 (C=O linker).

#### 2.5. Synthesis of Compound 4: Propargyl N-dodecylcarbamate

Triethylamine (1.05 equiv., 0.229 g, 2.27 mmol) and drop by drop propargyl chloroformate (1 equiv., 0.256 g, 2.16 mmol) were sequentially added to a solution of dodecylamine (1 equiv., 0.400 g, 2.16 mmol) in anhydrous DCM (6 mL) and under argon. The mixture was stirred for 3 h at 0 °C until the completion of the reaction, followed by concentration to dryness under vacuum. The resulting crude was purified by flash chromatography on a silica gel (petroleum ether/EtOAc, 90:10) to obtain the expected compound 4 as a colorless oil (0.333 g, 97%). **R<sub>f</sub>**: 0.61 (petroleum ether/EtOAc, 90:10). **<sup>1</sup>H NMR** (300 MHz, CDCl<sub>3</sub>) δ (ppm): 0.72–0.85 (m, 3H, CH<sub>3</sub> lipid), 1.19 (s, 18H, CH<sub>2</sub> lipid), 1.37–1.52 (m, 2H, CH<sub>2</sub>-CH<sub>3</sub> lipid), 2.40 (s, 1H, CH propargyl), 3.03–3.17 (m, 2H, CH<sub>2</sub>-NH lipid), 4.60 (s, 2H, CH<sub>2</sub> propargyl), 4.99–5.24 (bs, 1H, NH lipid). **<sup>13</sup>C NMR** (75.46 MHz, CDCl<sub>3</sub>) δ (ppm): 14.1 (CH<sub>3</sub> lipid), 22.7 (CH<sub>2</sub> lipid), 26.7 (CH<sub>2</sub> lipid), 29.3 (CH<sub>2</sub> lipid), 29.3 (CH<sub>2</sub> lipid), 29.5 (CH<sub>2</sub> lipid), 29.6 (CH<sub>2</sub> lipid), 29.6 (CH<sub>2</sub> lipid), 29.6 (CH<sub>2</sub> lipid), 29.8 (CH<sub>2</sub>-CH<sub>3</sub> lipid), 31.9 (CH<sub>2</sub> lipid), 41.2 (CH<sub>2</sub>-NH lipid), 52.2 (CH<sub>2</sub> propargyl), 74.4 (CH propargyl), 78.4 (C propargyl), 155.5 (C=O lipid).

#### 2.6. Synthesis of Compound 5: 3'-[3'-O-(tert-butyl dimethylsilyl)-5'-{4-[(dodecylcarbamoyloxy)methyl]-1H-1,2,3-triazol-1-yl}]-5'-deoxythymidin-3-yl] Methyl Propanoate

Compound 4 (1 equiv., 0.181 g, 0.68 mmol), copper (II) sulfate pentahydrate (0.1 equiv., 0.011 g, 0.07 mmol) and sodium ascorbate (0.2 equiv., 0.027 g, 0.14 mmol) were sequentially added to a solution of 3 (1 equiv., 0.316 g, 0.68 mmol) in a mixture of H<sub>2</sub>O/THF (tetrahydrofuran) (1:1, 5 mL). The mixture was stirred overnight at 60 °C until the completion of the reaction, followed by concentration to dryness under vacuum to obtain a green product. This was washed several times with EDTA (Ethylenediaminetetraacetic acid) until colorless organic phases were obtained, followed by concentration to dryness under vacuum. The resulting crude was purified by flash chromatography on a silica gel (toluene/acetone, 80:20) to obtain the expected compound 5 as a white powder (0.433 g, 87%). **R<sub>f</sub>**: 0.33 (toluene/acetone, 80:20). **<sup>1</sup>H NMR** (300 MHz, CDCl<sub>3</sub>) δ (ppm): 0.04–0.07 (m, 6H, CH<sub>3</sub>-Si), 0.78–0.92 (m, 12H, CH<sub>3</sub> lipid et <sup>t</sup>Bu), 1.20 (m, 18H, CH<sub>2</sub> lipid), 1.33–1.49 (m, 2H, CH<sub>2</sub>-CH<sub>3</sub> lipid), 1.84 (s, 3H, CH<sub>3</sub> thymidine), 2.00–2.77 (m, 2H, H<sub>2'</sub>), 2.58 (t, J = 7.2 Hz, 2H, H<sub>B</sub> linker), 3.03–3.14 (m, 2H, CH<sub>2</sub>-NH lipid), 3.62 (s, 3H, H<sub>C</sub> linker), 4.02–4.11 (m, 1H, H<sub>4'</sub>), 4.17 (t, J = 7.8 Hz, 2H, H<sub>A</sub> linker), 4.34–4.48 (m, 1H, H<sub>3'</sub>), 4.52–4.63 (m, 2H, H<sub>5'</sub>), 4.93–5.04 (m, 1H, NH lipid), 5.10 (s, 2H, O-CH<sub>2</sub> triazole), 6.15 (t, J = 6.6 Hz, 1H, H<sub>1'</sub>), 6.60 (s, 1H, H<sub>6</sub>), 7.66 (s, 1H, CH triazole). **<sup>13</sup>C NMR** (75.46 MHz, CDCl<sub>3</sub>) δ (ppm): −4.8 (CH<sub>3</sub>-Si), −4.6 (CH<sub>3</sub>-Si), 13.2 (CH<sub>3</sub> thymidine), 14.1 (CH<sub>3</sub> lipid), 17.8 (C<sub>q</sub> <sup>t</sup>Bu), 22.7 (CH<sub>2</sub> lipid), 25.7 (CH<sub>3</sub> <sup>t</sup>Bu), 26.7 (CH<sub>2</sub> lipid), 29.3 (CH<sub>2</sub> lipid), 29.3 (CH<sub>2</sub> lipid), 29.6 (CH<sub>2</sub> lipid), 29.6 (CH<sub>2</sub> lipid), 29.6 (CH<sub>2</sub> lipid), 29.8 (CH<sub>2</sub>-CH<sub>3</sub> lipid), 29.9 (CH<sub>2</sub> lipid), 31.9 (CH<sub>2</sub> lipid), 32.1 (CH<sub>2</sub>-B linker), 37.1 (CH<sub>2</sub>-A linker), 39.5 (C<sub>2'</sub>), 41.1 (CH<sub>2</sub>-NH lipid), 50.5 (C<sub>5'</sub>), 51.8 (CH<sub>3</sub>-C linker), 57.7 (O-CH<sub>2</sub> triazole), 71.7 (C<sub>3'</sub>), 83.9 (C<sub>4'</sub>), 86.0 (C<sub>1'</sub>), 110.8 (C<sub>5</sub>), 125.6 (CH triazole), 133.8 (C<sub>6</sub>), 143.6 (C triazole), 150.5 (C=O thymidine), 156.2 (C=O lipid), 162.9 (C=O thymidine), 171.6 (C=O linker). **HRMS** (ESI) [M + H<sup>+</sup>]: calcd = 735.44712, found = 735.44576.

#### 2.7. Synthesis of Compound 6: 3'-[3'-O-(tert-butyl dimethylsilyl)-5'-{4-[(dodecylcarbamoyloxy)methyl]-1H-1,2,3-triazol-1-yl}]-5'-deoxythymidin-3-yl] Propanoic Acid

Compound 5 (1 equiv., 0.431 g, 0.59 mmol) was dissolved in 1,4-dioxane (13 mL) before adding a solution of NaOH (1N) in MeOH (1.3 mL). The mixture was stirred overnight at room temperature until the completion of the reaction. The reaction mixture was treated with a solution of HCl (5%) to reach neutrality and then concentrated to dryness under vacuum. The resulting crude was purified by flash chromatography on

a silica gel (DCM/MeOH, 90:10) to obtain the expected compound **6** (0.310 g, 73%). **R<sub>f</sub>**: 0.26 (DCM/MeOH, 90:10). **<sup>1</sup>H NMR** (300 MHz, CDCl<sub>3</sub>) δ (ppm): −0.05–0.05 (m, 6H, CH<sub>3</sub>-Si), 0.73–0.85 (m, 12H, CH<sub>3</sub> lipid et <sup>t</sup>Bu), 1.10–1.27 (m, 18H, CH<sub>2</sub> lipid), 1.29–1.47 (m, 2H, CH<sub>2</sub>-CH<sub>3</sub> lipid), 1.79 (s, 3H, CH<sub>3</sub> thymidine), 2.07–2.21 (m, 2H, H<sub>2'</sub>), 2.37–2.51 (m, 2H, H<sub>B</sub> linker), 2.89–3.11 (m, 2H, CH<sub>2</sub>-NH lipid), 3.97–4.15 (m, 3H, H<sub>4'</sub> et H<sub>A</sub> linker), 4.30–4.43 (m, 1H, H<sub>3'</sub>), 4.50–4.59 (m, 2H, H<sub>5'</sub>), 5.07 (s, 2H, O-CH<sub>2</sub> triazole), 5.21–5.31 (m, 1H, NH lipid), 6.09 (t, *J* = 6.6 Hz, 1H, H<sub>1'</sub>), 6.61 (s, 1H, H<sub>6</sub>), 7.67 (s, 1H, CH triazole), 7.75–8.12 (bs, 1H, COOH linker). **<sup>13</sup>C NMR** (75.46 MHz, CDCl<sub>3</sub>) δ (ppm): −4.9 (CH<sub>3</sub>-Si), −4.8 (CH<sub>3</sub>-Si), 13.1 (CH<sub>3</sub> thymidine), 14.0 (CH<sub>3</sub> lipid), 17.7 (C<sub>q</sub> tBu), 22.6 (CH<sub>2</sub> lipid), 25.5 (CH<sub>3</sub> <sup>t</sup>Bu), 26.7 (CH<sub>2</sub> lipid), 29.2 (CH<sub>2</sub> lipid), 29.2 (CH<sub>2</sub> lipid), 29.3 (CH<sub>2</sub> lipid), 29.4 (CH<sub>2</sub> lipid), 29.5 (CH<sub>2</sub> lipid), 29.5 (CH<sub>2</sub>-CH<sub>3</sub> lipid), 29.8 (CH<sub>2</sub> lipid), 31.8 (CH<sub>2</sub> lipid), 33.6 (CH<sub>2</sub>-B linker), 38.0 (CH<sub>2</sub>-A linker), 39.2 (C<sub>2'</sub>), 41.0 (CH<sub>2</sub>-NH lipid), 50.6 (C<sub>5'</sub>), 57.6 (O-CH<sub>2</sub> triazole), 71.8 (C<sub>3'</sub>), 84.0 (C<sub>4'</sub>), 86.3 (C<sub>1'</sub>), 110.5 (C<sub>5</sub>), 125.3 (CH triazole), 133.8 (C<sub>6</sub>), 143.5 (C triazole), 150.4 (C=O thymidine), 156.1 (C=O lipid), 162.9 (C=O thymidine), 175.9 (C=O linker). **HRMS** (ESI) [M + H<sup>+</sup>]: calcd = 721.43147, found = 721.43198.

### 2.8. Synthesis of Compound 7: 2, 2', 3, 3', 4, 4', 6'-Hepta-O-(trimethylsilyl)-α,α'-D-trehalose

D-(+)-trehalose dihydrate (1 equiv., 0.500 g, 1.32 mmol) was co-evaporated to dryness under vacuum with anhydrous DMF (3 × 10 mL). Following this, *N,O*-bistrimethylsilylaceta mide (8.6 equiv., 2.78 mL, 11.37 mmol) and TBAF (Tetra-*n*-butylammonium fluoride) (0.06 equiv., 79 μL, 0.08 mmol) were sequentially added to a solution of the D-(+)-trehalose dihydrate dissolved in anhydrous DMF (4 mL). The completion of the reaction was reached by stirring the mixture overnight at room temperature. The mixture was then diluted in MeOH (60 mL) before the addition of K<sub>2</sub>CO<sub>3</sub> (0.11 equiv., 0.020 g, 0.145 mmol). It was then stirred 4 h at 0 °C, before a quenching of the reaction by the addition of NaHCO<sub>3</sub> (50 mL, aq.) and a dilution with water (30 mL). The aqueous phase was extracted 3 times with EtOAc (3 × 30 mL), prior to a drying over Na<sub>2</sub>SO<sub>4</sub> of the combined organic phases, and a concentration to dryness under vacuum. The expected compound **7** was obtained as a white powder by a purification using flash chromatography on a silica gel (petroleum ether/EtOAc/NEt<sub>3</sub>, 80:19:1) (0.530 g, 52%). **R<sub>f</sub>**: 0.42 (petroleum ether/EtOAc/NEt<sub>3</sub>, 80:19:1). **<sup>1</sup>H NMR** (300 MHz, MeOD) δ (ppm): 0.12–0.20 (m, 54H, 6 TMS), 1.90 (bs, 2H, OH), 3.48 (dd, 2H, *J* = 3.0 Hz, 9.3 Hz, H<sub>2</sub>, H<sub>2'</sub>), 3.49–3.52 (dd, 2H, H<sub>4</sub>, H<sub>4'</sub>), 3.65–3.71 (m, 4H, H<sub>6</sub>, H<sub>6'</sub>), 3.83–3.93 (m, 4H, H<sub>3</sub>, H<sub>3'</sub>, H<sub>5</sub>, H<sub>5'</sub>), 4.96 (d, 2H, H<sub>1</sub>, H<sub>1'</sub>). **<sup>13</sup>C NMR** (75.46 MHz, MeOD) δ (ppm): 0.3, 1.2, 1.6 (6 TMS), 61.7 (C<sub>6</sub>, C<sub>6'</sub>), 72.5, 74.4, 74.9 (C<sub>2</sub>, C<sub>2'</sub>, C<sub>3</sub>, C<sub>3'</sub>, C<sub>4</sub>, C<sub>4'</sub>), 74.0 (C<sub>5</sub>, C<sub>5'</sub>), 95.5 (C<sub>1</sub>, C<sub>1'</sub>).

### 2.9. Synthesis of Compound 8: 2,2',3,3',4,4',6'-Hepta-O-(trimethylsilyl)-α,α'-D-trehalos-6-yl 3-[3'-O-(tert-butylidimethylsilyl)-5'-4-[(dodecylcarbamoxy)methyl]-1H-1,2,3-triazol-1-yl]-5'-deoxythymidin-3-yl] Propanoate

Compound **7** (1 equiv., 0.126 g, 0.16 mmol), DCC (*N,N'*-Dicyclohexylcarbodiimide) (1.5 equiv., 0.050 g, 0.24 mmol) and DMAP (4-Dimethylaminopyridine) (0.5 equiv., 0.010 g, 0.08 mmol) were sequentially added to a solution of **6** (1.5 equiv., 0.175 g, 0.24 mmol) in anhydrous DCM (3 mL) and under argon. The mixture was stirred overnight at room temperature until the completion of the reaction. The precipitate was filtered and washed with DCM, followed by concentration to dryness of the filtrate under vacuum. The resulting crude was purified by flash chromatography on a silica gel (petroleum ether/EtOAc, 75:25) to obtain the expected compound **8** as a white powder (0.147 mg, 41%). **R<sub>f</sub>**: 0.49 (petroleum ether/EtOAc, 75:25). **<sup>1</sup>H NMR** (300 MHz, CDCl<sub>3</sub>) δ (ppm): −0.01–0.21 (m, 60H, CH<sub>3</sub>-Si et OTMS), 0.78–0.93 (m, 12H, CH<sub>3</sub> lipid et <sup>t</sup>Bu), 1.15–1.32 (m, 18H, CH<sub>2</sub> lipid), 1.36–1.51 (m, 2H, CH<sub>2</sub>-CH<sub>3</sub> lipid), 1.87 (s, 3H, CH<sub>3</sub> thymidine), 1.96–2.13 (m, 1H, H<sub>2'</sub>), 2.17–2.31 (m, 1H, H<sub>2'</sub>), 2.60–2.75 (m, 2H, H<sub>B</sub> linker), 3.04–3.16 (m, 2H, CH<sub>2</sub>-NH lipid), 3.34–3.51 (m, 4H, H<sub>A</sub> linker et H<sub>2</sub> trehalose, H<sub>2'</sub> trehalose), 3.60–3.74 (m, 2H, H<sub>6'</sub> trehalose), 3.77–4.33 (m, 10H, H<sub>4'</sub>, H<sub>6</sub> trehalose, H<sub>3</sub> trehalose, H<sub>3'</sub> trehalose, H<sub>4</sub> trehalose, H<sub>4'</sub> trehalose, H<sub>5</sub> trehalose, H<sub>5'</sub> trehalose et OH trehalose), 4.39–4.47 (m, 1H, H<sub>3'</sub>), 4.55–4.61 (m, 2H, H<sub>5'</sub>), 4.83–4.91 (d, 2H,

H<sub>1</sub> trehalose, H<sub>1'</sub> trehalose), 4.93–5.02 (m, 1H, NH lipid), 5.13 (s, 2H, O-CH<sub>2</sub> triazole), 6.19 (t,  $J = 6.6$  Hz, 1H, H<sub>1'</sub>), 6.63 (s, 1H, H<sub>6</sub>), 7.69 (s, 1H, CH triazole). <sup>13</sup>C NMR (75.46 MHz, CDCl<sub>3</sub>)  $\delta$  (ppm): −4.7 (CH<sub>3</sub>-Si), −4.5 (CH<sub>3</sub>-Si), 0.5 (OTMS), 1.2 (OTMS), 1.5 (OTMS), 13.3 (CH<sub>3</sub> thymidine), 14.5 (CH<sub>3</sub> lipid), 18.6 (C<sub>q</sub> <sup>t</sup>Bu), 23.6 (CH<sub>2</sub> lipid), 25.9 (CH<sub>3</sub> <sup>t</sup>Bu), 26.2 (CH<sub>2</sub> lipid), 26.6 (CH<sub>2</sub> lipid), 27.7 (CH<sub>2</sub> lipid), 30.2 (CH<sub>2</sub> lipid), 30.3 (CH<sub>2</sub> lipid), 30.6 (CH<sub>2</sub> lipid), 30.7 (CH<sub>2</sub> lipid), 32.9 (CH<sub>2</sub>-CH<sub>3</sub> lipid), 33.1 (CH<sub>2</sub>-B linker), 34.6 (CH<sub>2</sub> lipid), 38.2 (CH<sub>2</sub>-A linker), 40.2 (C<sub>2'</sub>), 41.7 (CH<sub>2</sub>-NH lipid), 52.0 (C<sub>5'</sub>), 58.2 (O-CH<sub>2</sub> triazole), 61.6 (C<sub>6'</sub> trehalose), 64.9 (C<sub>6</sub> trehalose), 71.6, 72.4 (C<sub>2</sub> trehalose, C<sub>2'</sub> trehalose), 73.0 (C<sub>5'</sub> trehalose), 73.5 (C<sub>3'</sub>), 73.7 (C<sub>5</sub> trehalose), 73.8, 74.4, 74.6, 74.7 (C<sub>3</sub> trehalose, C<sub>3'</sub> trehalose, C<sub>4</sub> trehalose, C<sub>4'</sub> trehalose), 85.9 (C<sub>4'</sub>), 88.2 (C<sub>1'</sub>), 95.2, 95.4 (C<sub>1</sub> trehalose, C<sub>1'</sub> trehalose), 111.0 (C<sub>5</sub>), 126.7 (CH triazole), 136.5 (C<sub>6</sub>), 144.7 (C triazole), 151.6 (C=O thymidine), 158.1 (C=O lipid), 164.8 (C=O thymidine), 172.6 (C=O linker). HRMS (ESI) [M + H<sup>+</sup>]: calcd = 1477.77427, found = 1477.77674.

### 2.10. Synthesis of Compound 9 (GNL):

#### 5'-[4-[(Dodecylcarbamoyloxy)methyl]-1H-1,2,3-triazol-1-yl]-5'-deoxythymidin-3-yl Propanoate

Dowex 50WX2-100 ion exchange resin (0.350 g) was added to a solution of **8** (1 equiv., 0.105 g, 0.07 mmol) in MeOH (20 mL). The mixture was stirred for 15 min at room temperature until the completion of the reaction. The mixture was then filtered and the filtrate was evaporated under vacuum. Purification of compound **9'** (0.062 g, 85%) was not necessary and it was directly engaged in the next reaction after drying. TBAF (1 equiv., 62  $\mu$ L, 0.06 mmol) was added to a solution of **9'** (1 equiv., 0.062 g, 0.06 mmol) in anhydrous THF (3 mL) and under argon at 0 °C. The mixture was stirred for 2 h at 0 °C until the completion of the reaction. The reaction was then quenched by the addition of water (5 mL, aq.). The expected compound **9** (white powder) was obtained after three extractions of the aqueous phase with DCM (3  $\times$  10 mL), drying of the combined organic phases over Na<sub>2</sub>SO<sub>4</sub>, a concentration to dryness under vacuum and a purification of the resulting crude by flash chromatography on a silica gel (DCM/MeOH/Water, 80:18.5:1.5) (0.029 g, 52%). R<sub>f</sub>: 0.31 (petroleum ether/EtOAc/NEt<sub>3</sub>, 80:18.5:1.5). <sup>1</sup>H NMR (300 MHz, MeOD)  $\delta$  (ppm): 0.84–0.98 (m, 3H, CH<sub>3</sub> lipid), 1.18–1.40 (m, 18H, CH<sub>2</sub> lipid), 1.41–1.55 (m, 2H, CH<sub>2</sub>-CH<sub>3</sub> lipid), 1.92 (s, 3H, CH<sub>3</sub> thymidine), 2.21–2.39 (m, 2H, H<sub>2'</sub>), 2.65 (t,  $J = 7.2$  Hz, 2H, H<sub>B</sub> linker), 2.99–3.09 (m, 2H, CH<sub>2</sub>-NH lipid), 3.25–3.37 (m, 6H, H<sub>2</sub> trehalose, H<sub>2'</sub> trehalose, H<sub>3</sub> trehalose, H<sub>3'</sub> trehalose, H<sub>4</sub> trehalose et H<sub>4'</sub> trehalose), 3.45 (q,  $J = 3.9$  Hz, 9.9 Hz, 2H, H<sub>6'</sub> trehalose), 3.70–3.80 (m, 1H, H<sub>5'</sub> trehalose), 3.97–4.05 (m, 1H, H<sub>5</sub> trehalose), 4.11–4.36 (m, 5H, H<sub>4'</sub>, H<sub>A</sub> linker, H<sub>6</sub> trehalose), 4.36–4.44 (m, 1H, H<sub>3'</sub>), 4.65–4.79 (m, 2H, H<sub>5'</sub>), 4.83–5.02 (d, 2H, H<sub>1</sub> trehalose, H<sub>1'</sub> trehalose), 5.10 (s, 2H, O-CH<sub>2</sub> triazole), 6.15 (t,  $J = 6.9$  Hz, 1H, H<sub>1'</sub>), 7.23 (s, 1H, H<sub>6</sub>), 8.00 (s, 1H, CH triazole). <sup>13</sup>C NMR (75.46 MHz, MeOD)  $\delta$  (ppm): 13.1 (CH<sub>3</sub> thymidine), 14.3 (CH<sub>3</sub> lipid), 23.2 (CH<sub>2</sub> lipid), 25.4 (CH<sub>3</sub> <sup>t</sup>Bu), 29.6 (CH<sub>2</sub> lipid), 29.6 (CH<sub>2</sub> lipid), 29.9 (CH<sub>2</sub> lipid), 30.0 (CH<sub>2</sub> lipid), 30.2 (CH<sub>2</sub> lipid), 30.2 (CH<sub>2</sub> lipid), 30.2 (CH<sub>2</sub> lipid), 32.4 (CH<sub>2</sub>-CH<sub>3</sub> lipid), 32.8 (CH<sub>2</sub>-B linker), 34.6 (CH<sub>2</sub> lipid), 34.8 (CH<sub>2</sub>-A linker), 37.8 (C<sub>2'</sub>), 39.4 (CH<sub>2</sub>-NH lipid), 51.9 (C<sub>5'</sub>), 62.2 (O-CH<sub>2</sub> triazole), 63.2 (C<sub>6'</sub> trehalose), 64.9 (C<sub>6</sub> trehalose), 69.2, 70.6 (C<sub>2</sub> trehalose, C<sub>2'</sub> trehalose), 70.9 (C<sub>5'</sub> trehalose), 71.2 (C<sub>3'</sub>), 71.5 (C<sub>5</sub> trehalose), 72.3, 73.0, 73.6, 73.8 (C<sub>3</sub> trehalose, C<sub>3'</sub> trehalose, C<sub>4</sub> trehalose, C<sub>4'</sub> trehalose), 84.6 (C<sub>4'</sub>), 87.3 (C<sub>1'</sub>), 94.3, 95.5 (C<sub>1</sub> trehalose, C<sub>1'</sub> trehalose), 110.8 (C<sub>5</sub>), 125.3 (CH triazole), 136.9 (C<sub>6</sub>), 145.1 (C triazole), 151.2 (C=O thymidine), 155.6 (C=O lipid), 164.2 (C=O thymidine), 172.3 (C=O linker). HRMS (ESI) [M + H<sup>+</sup>]: calcd = 931.45356, found = 931.64586.

### 2.11. Synthesis of Compound 10 (dATr): 6,6'-Bis-O-dodecanoyl- $\alpha,\alpha'$ -D-trehalose

Compound **7** (1 equiv., 0.200 g, 0.26 mmol), DCC (2 equiv., 0.106 g, 0.52 mmol) and DMAP (0.5 equiv., 0.016 g, 0.13 mmol) were sequentially added to a solution of lauric acid (2 equiv., 0.104 g, 0.52 mmol) in anhydrous DCM (3 mL) and under argon. The mixture was stirred overnight at room temperature until the completion of the reaction. The precipitate was filtered and washed with DCM, followed by concentration to dryness of the filtrate under vacuum. The resulting crude was purified by flash chromatography

on a silica gel (petroleum ether/EtOAc, 75:25) to obtain the expected compound **7'** as a white powder (0.254 mg, 86%). Next, Dowex 50WX2-100 ion exchange resin (0.700 g) was added to a solution of **8'** (1 equiv., 0.254 g, 0.22 mmol) in MeOH (40 mL). The mixture was stirred for 15 min at room temperature until the completion of the reaction. The mixture was then filtered and the filtrate was evaporated under vacuum. Purification of compound **10** (0.143 g, 91%) was not necessary and it was directly engaged in the next reaction after drying. **R<sub>f</sub>**: 0.49 (petroleum ether/EtOAc, 75:25). <sup>1</sup>H NMR (300 MHz, MeOD) δ (ppm): 0.70–0.82 (m, 3H, CH<sub>3</sub> lipid), 1.03–1.25 (m, 32H, CH<sub>2</sub> lipid), 1.28–1.42 (m, 4H, CH<sub>2</sub>-CH<sub>3</sub> lipid), 3.15–3.26 (m, 4H, CH<sub>2</sub>-C=O lipid), 3.50 (dd, 2H, *J* = 3.1 Hz, 9.2 Hz, H<sub>2</sub>, H<sub>2'</sub>), 3.49–3.58 (m, 2H, H<sub>4</sub>, H<sub>4'</sub>), 3.63–3.70 (m, 4H, H<sub>6</sub>, H<sub>6'</sub>), 3.83–3.90 (m, 2H, H<sub>3</sub>, H<sub>3'</sub>), 3.92–4.02 (m, 2H, H<sub>5</sub>, H<sub>5'</sub>), 4.96 (d, 2H, H<sub>1</sub>, H<sub>1'</sub>). <sup>13</sup>C NMR (75.46 MHz, MeOD) δ (ppm): 13.8 (CH<sub>3</sub> lipid), 20.5 (CH<sub>2</sub> lipid), 24.7 (CH<sub>2</sub> lipid), 30.1 (CH<sub>2</sub> lipid), 30.5 (CH<sub>2</sub> lipid), 30.6 (CH<sub>2</sub> lipid), 30.6 (CH<sub>2</sub> lipid), 30.9 (CH<sub>2</sub> lipid), 30.9 (CH<sub>2</sub>-CH<sub>3</sub> lipid), 31.1 (CH<sub>2</sub> lipid), 31.5 (CH<sub>2</sub> lipid), 61.7, 61.8 (C<sub>6</sub>, C<sub>6'</sub>), 71.3, 72.5, 74.4 (C<sub>2</sub>, C<sub>2'</sub>, C<sub>3</sub>, C<sub>3'</sub>, C<sub>4</sub>, C<sub>4'</sub>), 74.9 (C<sub>5</sub>, C<sub>5'</sub>), 95.5 (C<sub>1</sub>, C<sub>1'</sub>).

### 2.12. General Procedure for Nanoparticles and Solid Lipid Nanoparticles Preparation

The PLGA was purchased from Sigma-Aldrich (Resomer<sup>®</sup> RG 503H PLGA; lactide-glycoside ratio of 50:50; molecular weight from 24,000 to 38,000). The nanoprecipitation protocol was adapted from a previous study to prepare NP suspensions [19,34]. Briefly, 31 mg of Resomer<sup>®</sup> RG 503H PLGA was dissolved in 3.1 mL of tetrahydrofuran (THF; Sigma-Aldrich). Under sonication (37Hz, 100%, 3 min), 200 μL of the previous solution was quickly added to 20 mL of deionized water. The resulting NP suspension was then slowly concentrated by centrifugation using 10 kDa centrifugal filters (Merck Millipore, Saint Quentin Fallavier, France, Amicon Ultra centrifugal Filter) for 21 min at 5000 RPM (Centrifuge 5804 R, Eppendorf). Once the supernatant had been collected, the resulting suspension was ready for use (typical concentration of NPs ~ 0.2 mg·mL<sup>-1</sup>). A rapid mixing protocol was adapted from the literature to prepare the NP suspension. 500 μL of the previously prepared stock solution was simultaneously injected (3 mL·min<sup>-1</sup>) with 1.5 mL of deionized water (9 mL·min<sup>-1</sup>) using syringe pumps (kdScientific, Holliston, MA, USA). The obtained PLGA NP suspension was concentrated to a typical concentration of 2.5 mg·mL<sup>-1</sup>. For the control condition, PLGA NPs loaded with Nile Red fluorophore (Sigma-Aldrich, St. Louis, MO, USA 19123) were formulated as previously described, except that 0.9 mg of Nile Red was added to the polymer stock solution. **F2** and **F3** were formulated similarly, except that 15% (*w/w*) of **dATr** or **GNL** were introduced into the stock solution (typical final concentration in trehalose 0.4 μM). For all experiments, PLGA NP suspensions were prepared extemporaneously.

### 2.13. Nanoparticle and Solid Lipid Nanoparticle Characterization and Stability Evaluation

Granulometric profile of NPs and SLNs were acquired by Dynamic Light Scattering (DLS), using Malvern Instruments (Zetasizer Nano ZS, Palaiseau, France). NPs/SLNs were diluted at 1:1000 (*v/v*), then the average size and the polydispersity index were obtained in triplicate at 25 °C. To determine the Zeta potential, NPs/SLNs, at the same dilution, were analyzed using a Zetasizer Nano ZS coupled with Folded Capillary Cell (DTS1060). Short-term stability assessment was performed for a period of one month by visually checking the lack of creaming or phase separation and monitoring the size and zeta potential. Transmission electron microscopy was carried out using a Hitachi (Tokyo, Japan) coupled to an ORIUS SC1000 11MPX (Gatan, Pleasanton, CA, USA). All samples were deposited on carbon-coated grids (Delta Microscopies, Mauressac, France) and dried after 3 min of contact. A staining procedure using uranylless (Delta Microscopies, Mauressac, France) or nanotungstene was used.

#### 2.14. Quantification of the Free GNL by Enzymatic Assay

Quantification of the free GNL in the suspensions of trehalose derivative-loaded NPs was performed using the Megazyme microplate assay procedure (Trehalose Assay Kit, Megazyme, Bray, Ireland) [34]. Briefly, trehalose standard solutions (concentration between 25 and 100  $\mu\text{M}$ ) were prepared and 20  $\mu\text{L}$  of each was used for the calibration curve. To these 20  $\mu\text{L}$  were added 200  $\mu\text{L}$  of deionized water, 20  $\mu\text{L}$  of solution 1 (buffer), 10  $\mu\text{L}$  of solution 2 (containing both nicotinamide adenine dinucleotide phosphate ( $\text{NADP}^+$ ) and adenosine 5' triphosphate) and 2  $\mu\text{L}$  of solution 3 (containing the hexokinase and glucose-6-phosphate dehydrogenase). The solutions were mixed and the absorbance was measured at 340 nm ( $\text{abs}_0$ ) before addition to the trehalase medium. The next step was the addition of 2  $\mu\text{L}$  of suspension 4, containing trehalase, to the wells. The 96-well plate was shaken and incubated for 8 min at room temperature before the absorbance of the different solutions at 340 nm ( $\text{abs}_1$ ) was read. The calibration curve was thus obtained by representing the background-corrected absorbance ( $\text{abs}_1 - \text{abs}_0$ ) as a function of the trehalose concentration. For the quantification of the NP samples, the same protocol was used except for the direct use of 220  $\mu\text{L}$  of suspension instead of 20  $\mu\text{L}$  of standard and 200  $\mu\text{L}$  of deionized water, to ensure absorbances included in the calibration range.

#### 2.15. Encapsulation Efficiency and Drug Loading

For the determination of the encapsulation efficiency (EE) and the drug loading (DL) of PLGA NPs, GNL quantification was achieved by UV-Vis spectroscopy (Jasco V-630, France) using a standard calibration curve of GNL dissolved in methanol (between 5 and 40  $\mu\text{g}\cdot\text{mL}^{-1}$ ; absorbance at 266.5 nm). Equation (1) was used, where  $y$  is the absorbance value and  $x$  the GNL concentration. The standard calibration curve was linear over the range of 5–40  $\mu\text{g}\cdot\text{mL}^{-1}$  with  $r^2 = 0.9993$ . The amount of encapsulated GNL in the PLGA NPs (also called DL) was calculated from the mass of the incorporated drug, using Equation (2):

$$y = 0.0088x + 0.1572 \quad (1)$$

$$\text{DL} = \frac{\text{Amount of GNL in NPs}}{\text{Amount of GNL loaded NPs}} \times 100 \quad (2)$$

The drug EE was defined as the ratio of the mass of the encapsulated drug over the mass of the drug used for the formulation, using the following equation:

$$\text{EE} = \frac{\text{Amount of encapsulated GNL}}{\text{Amount of GNL used for NP formulation}} \times 100 \quad (3)$$

The drug EE and the DL efficiency were calculated using Equations (1)–(3).

#### 2.16. Infrared Analyses

Spectra of PLGA, GNL, F1 and F3 were acquired using an FT-IR spectrometer (FT-IR 4600, Jasco Inc., Tokyo, Japan) controlled by spectra manager software. Samples (3 mg) were mixed with 300 mg of KBr powder and then compressed with a mechanical die press to obtain translucent pellets. All spectra were recorded after averaging 16 accumulations with 8  $\text{cm}^{-1}$  resolution between 4000  $\text{cm}^{-1}$  and 450  $\text{cm}^{-1}$ . Background was performed on the atmosphere and subtracted to all acquisitions. All spectra were acquired in the transmittance mode. IR data were processed using spectra manager for IR spectra and IR derivatives (Savitzky–Golay: derivative order 1, polynome order 2 and window of 7 points).

#### 2.17. Cell Culture and Cell Viability Assay

Human neuroblastoma cell lines (BE(2)-M17) from ATCC (CRL-2267) were grown in Opti-MEM (Life Technologies, Carlsbad, CA, USA; 31985-047) supplemented with 10% fetal bovine serum (Sigma-Aldrich) and 1% penicillin/streptomycin. All NP and SLN suspensions were used as freshly prepared on cells grown at 70% to 80% confluence. Cells

were exposed at 0.5  $\mu\text{L}$  of loaded NPs and SLNs for 24 h or 48 h, and each experiment was performed at least in triplicate. MTS assay (ATCC/LGC Promochem, Molsheim, France) estimated cell viability using the manufacturer instructions.

#### 2.18. Western Blot Analysis

BE(2)-M17 cells were seeded on 6-well plates (NUNC) and grown to 70–80% confluence per well before being treated with **F1**, **F2**, **F3**, **F4** and molecular trehalose as control (concentration of 0.4  $\mu\text{M}$ ). The cells were then transferred to Eppendorf tubes before centrifugation for 5 min at 3000 rpm and 4 °C. The supernatant was removed before the dropwise addition of 50  $\mu\text{L}$  of P/X solution (P/X = 1.5 mL RB1X, 0.450 mL P4X, 0.050 mL dithiothreitol (DTT)) under mechanical agitation. The samples were then incubated for 5 min at 100 °C. Protein samples were loaded into 18% acrylamide gels and separated by SDS-PAGE (sodium dodecyl sulphate-polyacrylamide gel electrophoresis) before transfer to a nitrocellulose membrane (0.2  $\mu\text{m}$ —Biorad—USA). The membranes were then blocked in 5% PBS (phosphate-buffered saline)-milk buffer before overnight incubation at 4 °C with rabbit anti-LC3 (light chain 3) primary antibody (1/1000°, Novus Biological, Littleton, CO, USA #NB100-2220). An incubation with mouse anti-actin antibody (1/5000°, Sigma) served as a loading control. The appropriate secondary antibodies were then used before revelation with the revelation kit (Super Signal West Pico Chemiluminescent kit—Immobilon Western, Chemiluminescent HRP substrate, Millipore). Chemiluminescence images were acquired using a ChemiDoc + XRS analysis system (BioRad, Hercules, CA, USA). The signal per well was quantified using ImageJ software and normalized by actin before statistical analysis.

#### 2.19. Immunostaining and Imaging

Extemporaneous NP suspensions were used for all experiments. In the case of Nile Red-loaded NPs internalization and colocalization imaging assays, BE(2)-M17 cells were replated in 6-well plates (NUNC) with coverslips after trypsinization, and allowed growing at 70% to 80% confluence per well. They were then exposed to the tested formulations for 24 h at 37 °C. The final concentration of NPs in each well was set at  $\sim 3 \mu\text{g}\cdot\text{mL}^{-1}$  for **F5**. The cell fixation was performed using 4% paraformaldehyde for 20 min at 4 °C, prior to the washing step with PBS 1X solution. A mixture, composed of 225  $\mu\text{L}$  of triton, 450  $\mu\text{L}$  of normal goat serum and 5 mL of PBS 1X, was added for cell permeabilization and blocking steps. The LAMP2 (Mx, H4B4) antibodies and their appropriate secondary antibodies conjugated with GAM 488 (Life Technologies) were used to mark the lysosomes overnight at 4 °C and for staining, respectively. The cells were incubated with 8  $\mu\text{M}$  Hoechst dye (ThermoFisher Scientific, Waltham, MA, USA, #3342) (8 min; room temperature) to stain cytoplasm and nuclei, prior to mounting. After an air-drying step, slices were mounted on #1.5 coverslips using Dako fluorescent mounting medium, then left overnight in darkness to dry. A Leica TCS SP8 laser scanning confocal microscope (Leica Microsystems, Wetzlar, Germany) combined with a 63X Plan Apo CS oil immersion objective was used to acquire image stacks (pixel size  $\sim 100 \text{ nm}$ ; z-step 0.3  $\mu\text{m}$ ). Nile Red was observed in a detection window between 570 and 590 nm after an excitation at 568 nm (DPSS laser). For lysosomes, the excitation was performed at 488 nm (argon laser) and the detection within a window between 545 and 605 nm. In parallel, the untreated cells were required for autofluorescence controls using the previously described parameters. LAS AF v2.6 acquisition software implemented with HCS-A module (Leica Microsystems) was used for image analyses. The relative intensity of Nile Red to cell surface was determined using Definiens XD Developer v2.5 software (Definiens). The images were analyzed with the ImageJ (NIH, Bethesda, MD, USA; Fiji) software for colocalization, fluorescence profiles, orthogonal projections and maximal intensity projections.

### 2.20. GFP-LC3 Reporter Autophagy Assay

To assess autophagy activity, the green fluorescent protein (GFP)-LC3 reporter was used as previously described [29,35]. Briefly, a BE(2)-M17 cell line was plated on coverslips in 12-well plates which were transfected with mCherry-GFP-LC3 plasmid at 1.6  $\mu\text{g}$  DNA using polyethylenimine (PEI)-mediated transfection. Cells were maintained for 24 h at 37 °C in 5% CO<sub>2</sub> before being treated with unloaded or loaded NPs or SLNs for 24 h at 1:1000. Cell coverslips were fixed at 4 °C for 20 min using 4% paraformaldehyde, followed by 3 washing steps of 5 min with PBS 1X. The final step consisted in a staining using DAPI solution (10  $\mu\text{M}$ ; Invitrogen, Waltham, MA, USA) for 8 min prior to long washes in PBS 1X solution. Mounting solution (Dako) was used to mount the coverslips onto slides, and images were obtained using a wide-field Olympus Epifluorescent Microscope (BX3-CBH) coupled with a Hamamatsu camera (ORCA-Flash 4.0 LT). Images were deconvolved using the cellSens Dimension software. Image analysis was performed using Fiji/ImageJ software.

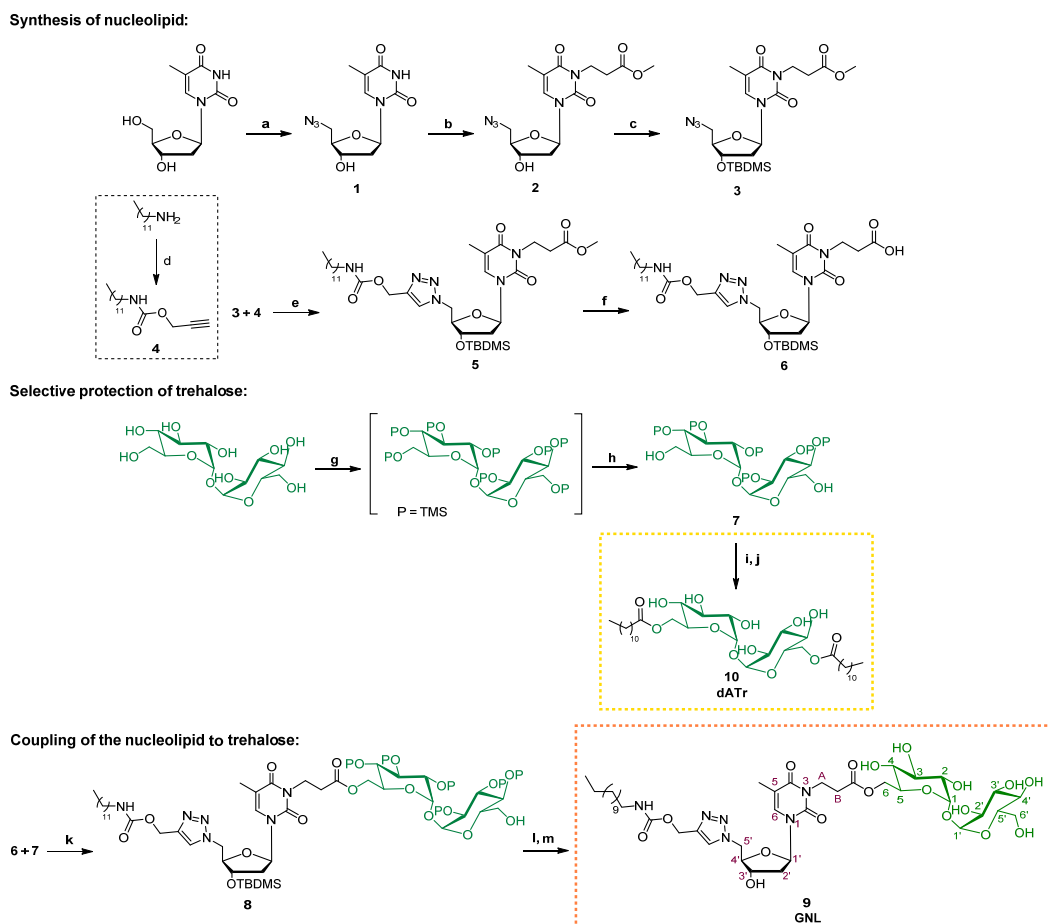
### 2.21. Statistical Analysis

Statistical analyses were performed using GraphPad Prism 6 software. In the case of functional assays, a one-way analysis of variance (ANOVA) was used to evaluate the data statistical significance prior to a Tukey's multiple comparison test. A significant difference was highlighted by  $p < 0.05$ . Data appear as estimation graphics called 'Gardner-Altman plots': in the top graph, the data from UT (untreated), F1, F2, F3 and F4 groups are presented as scatter plots showing the observed values, along with the above-defined descriptive statistics (mean  $\pm$  standard deviation). Below each graph, a contrast graph using the difference axis to display an effect size, here the mean difference. Vertically aligned with the mean of the UT group, the mean difference is indicated by the black circle. The 95% confidence interval (CI) of the mean difference is illustrated by the black vertical line. The curve indicates the resampled distribution of the effect size, given the observed data.

## 3. Results and Discussion

### 3.1. Design and Synthesis of Glyconucleolipidic Platforms

Two original compounds, a diacyl trehalose derivative (dATr, compound 10) and a glyconucleolipid (GNL, compound 9) composed of a single C12 lipid chain featuring trehalose as the carbohydrate moiety, were designed and synthesized (Scheme 1). GNL was synthesized by a ten-step synthesis route beginning with the functionalization of commercially available thymidine. In the first step, an azide group was introduced at the 5' position of the nucleoside through an Appel reaction, followed by a nucleophilic displacement of the bromine atom with NaN<sub>3</sub> to form the azidothymidine 1. The linker, coupling the NL moiety to trehalose, was added by a Michael reaction to form 2. After protecting the 3' position of thymidine, 3 was submitted to a CuAAC (Copper(I)-catalysed alkyne-azide cycloaddition) reaction with the previously prepared propargylated lipid chain 4 to give the corresponding 1,2,3-triazole derivative 5. The latter was saponified in basic medium, followed by esterification with the per-silylated trehalose 7, leading to compound 8. NLs were coupled to trehalose through an ester moiety, allowing its enzymatic release in neuronal cells once transportation through the lipid bilayers had been achieved. Deprotection of the silyl groups under acidic conditions yielded the final GNL structure. Compound 10 (dATr) was obtained by a selective protection of trehalose dihydrate 7, first followed by an esterification step to append the lauric chain and then followed by a deprotection step by means of Dowex 50WX2-100 ion exchange resin.



**Scheme 1. Synthetic route leading to GNL and trehalose derivative.** Reagents and conditions: **a**—PPh<sub>3</sub> (1.2 equiv.), NaN<sub>3</sub> (5 equiv.), CBr<sub>4</sub> (1.2 equiv.), anhydrous DMF, 24 h, RT, 74%; **b**—DBU (1.55 equiv.), methyl acrylate (1.55 equiv.), anhydrous DMF, 16 h, 60 °C, 66%; **c**—TBDMSCl (1.2 equiv.), imidazole (1.2 equiv.), anhydrous DMF, 15 h, RT, 86%; **d**—triethylamine (1.05 equiv.), propargyl chloroformate (1 equiv.), anhydrous DCM, 3 h, 0 °C, 97%; **e**—CuSO<sub>4</sub>, 5H<sub>2</sub>O (0.1 equiv.), sodium ascorbate (0.2 equiv.), THF/H<sub>2</sub>O (1:1), 15 h, 60 °C, 87%; **f**—NaOH (1N) in anhydrous methanol, anhydrous 1,4-dioxane, 15 h, RT, 73%; **g**—N,O-bis(trimethylsilyl)acetamide (8.6 equiv.), TBAF (0.06 equiv.), anhydrous DMF, 15 h, RT; **h**—K<sub>2</sub>CO<sub>3</sub> (0.11 eq.), anhydrous MeOH, 4 h, 0 °C, 52%; **i**—lauric acid (2 equiv.), DCC (2 equiv.), DMAP (0.5 equiv.), anhydrous DCM, 16 h, RT, 86%; **j**—Dowex 50WX2-100, anhydrous MeOH, 30 min., RT, 91%; **k**—nucleolipid (1.5 equiv.), DCC (1.5 equiv.), DMAP (0.5 equiv.), anhydrous DCM, 16 h, RT, 41%; **l**—Dowex 50WX2-100, anhydrous MeOH, 15 min, RT, 85%; **m**—TBAF (1 equiv.), anhydrous THF, 2h, 0 °C, 52%.

### 3.2. Physico-Chemical Characterization of PLGA Nanoparticles and Solid Lipid Nanoparticles

To evaluate either the added value to link trehalose to a NL or the PLGA NPs as a nanocarrier, five formulations were prepared. First, we used unloaded PLGA NPs (**F1**) as a control. Second, **dATr** was formulated into PLGA NPs, named **dATr**-loaded PLGA NPs (**F2**) and **GNL** was also formulated into PLGA NPs, described as **GNL**-loaded PLGA NPs (**F3**). By comparing **F2** and **F3**, we were able to gain insight into the contribution of NLs. Third, to assess whether a PLGA-free formulation was appropriate as a PLGA alternative, we took advantage of the self-assembling properties of **GNLs** to formulate them into SLNs [16,17] (**F4**). Finally, Nile Red-loaded PLGA NPs (**F5**) were prepared as an experimental readout to evaluate exclusively the internalization into neuronal cells (Figure 1).

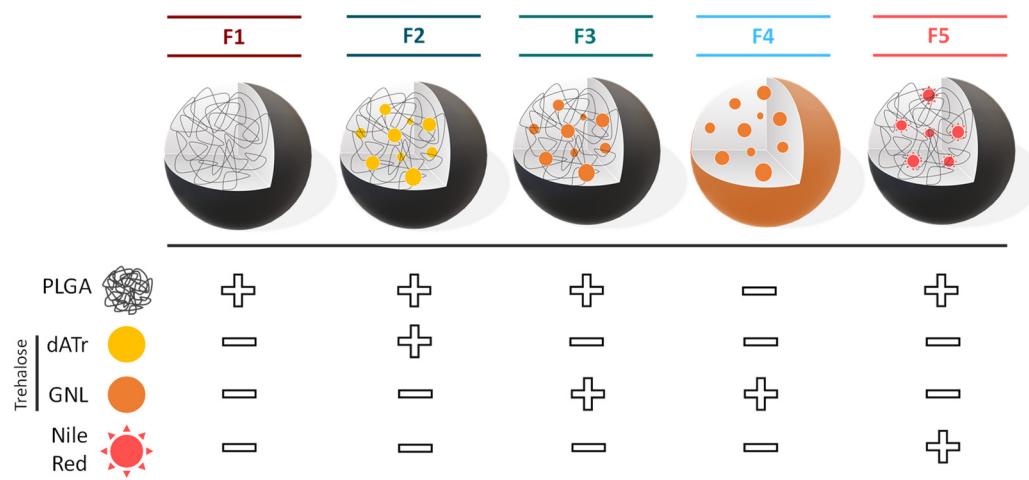


**Figure 1.** Schematic illustration of the nanoparticle compositions (+: presence of the compound; -: absence of the compound).

These nanovectors were first obtained by nanoprecipitation, and then by rapid mixing. Nanoprecipitation requires the addition of two miscible solvents, in this case THF and water, and results in the spontaneous formation of NPs on phase separation. With dissolved PLGA and active compounds (for loaded NPs), the organic phase was added dropwise to the aqueous medium under sonication. Once the nanocarriers were formed, the particle dispersions were further processed to purify and concentrate them through THF rotary evaporation and dialysis. The main drawback of this method was the loss of product due to the aggregation of PLGA during the process, and therefore, the low yield of production. On the other hand, rapid mixing involves the simultaneous injection of an organic phase (THF) and the aqueous medium using a syringe pump followed by a T-junction mixing [36]. The self-assembly of smaller NPs is thus produced by a supersaturation of PLGA and/or GNL in the medium, induced by the rapid increase in the polarity of the two miscible phases [36]. Compared to nanoprecipitation, rapid mixing has multiple advantages, such as quicker formulation of smaller nano-objects, allowing them to be obtained in 15 min instead of 45 min in the case of nanoprecipitation, and at a higher concentration ( $0.2 \text{ mg}\cdot\text{mL}^{-1}$  of NPs using nanoprecipitation versus  $2.5 \text{ mg}\cdot\text{mL}^{-1}$  using rapid mixing). Both trehalose derivatives were successfully incorporated into PLGA NPs or able to form SLNs. Therefore, three different formulations (F1, F2, F3) were prepared by both nanoprecipitation and rapid mixing to observe the process impact on the physico-chemical characteristics (size, polydispersity index (monodisperse suspension under 0.2) and zeta potential) (Table 1).

**Table 1.** Physicochemical properties of GLN nanoformulation function of the formulation process.

	F1	F2	F3	F4
Nano-precipitation	Diameter (nm)	$182.0 \pm 0.8$	$190.7 \pm 1.8$	$180.4 \pm 1.4$
	Polydispersity index	0.144	0.135	0.174
	$\zeta$ -potential (mV)	$-31.8 \pm 9.6$	$-45.4 \pm 1.6$	$-58.1 \pm 0.9$
Rapid mixing	Diameter (nm)	$97.6 \pm 17.2$	$156.2 \pm 5.6$	$167.2 \pm 2.4$
	Polydispersity index	0.147	0.198	0.202
	$\zeta$ -potential (mV)	$-47.3 \pm 2.0$	$-38.9 \pm 8.9$	$-35.1 \pm 0.6$

A significant decrease (student's test,  $p < 0.05$ ) in the mean diameter was observed for the three formulations (F1/F2/F3) using rapid mixing after dialysis. NPs with particle sizes below 200 nm were obtained, allowing membrane and biological barrier passage, as well as an increase in the half-life, crucial parameters for biomedical applications [37,38].

Another advantage of this approach was obtaining new nano-objects only made of **GNL**, i.e., SLN. These were formulated following the same protocol as the PLGA NPs, except for the polymer addition phase. These SLNs with a diameter close to PLGA-based NPs ( $120.4 \pm 1.4$  nm vs.  $167.2 \pm 2.4$  nm) had a surface charge of  $-16.2 \pm 1.7$  mV. The colloidal stability of the formulations obtained by rapid mixing was evaluated at 4 °C (storage condition) and 37 °C (use condition). In terms of diameter (Figure 2A), the objects were stable for at least 20 days at 4 °C, whereas at 37 °C, a destabilization, characterized by an increase in the diameter (10-fold), polydispersity (Figure 2B) and a modification of the zeta potential (Figure 2C), were observed from 10 days. Interestingly enough, the size of SLNs remained stable despite low surface loading (Figure 2A,C). This tendency may be due to the particular structure of SLNs based on physical interactions. Moreover, the in vitro biological analyses were carried out only during 3 days, ensuring the object stability.

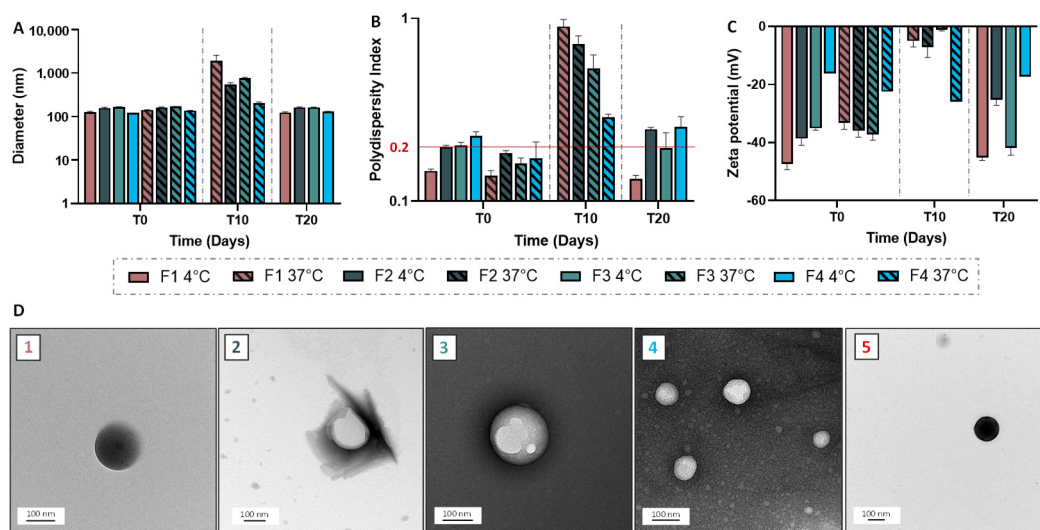


**Figure 2. Physicochemical characterization of the rapid mixing formulations.** Evolution of (A) the diameter, (B) polydispersity index (Pdl), and (C)  $\zeta$ -potential of F1 (red), F2 (dark blue), F3 (green), and F4 (cyan) overtime at 4 °C and 37 °C. (D) TEM images of (1) F1, (2) F2, (3) F3, (4) F4 and (5) F5 prepared by rapid mixing.

To dig deeper into the characterization of these nano-objects, two techniques were used: transmission electron microscopy (TEM) and infrared (IR) spectroscopy. The first one confirmed the size of the particles and their spherical shape (Figure 2D). The advantage of this study was obvious in the case of F5. Indeed, the study by DLS of this formulation containing Nile Red was not possible owing to the similarity in color between the chromophore and the laser used. TEM was, therefore, able to overcome this limit, allowing the observation of spherical objects with an average diameter of  $118.8 \pm 25.8$  nm consistent with the results obtained for other PLGA NPs. The second confirmed the presence of **GNL** in the NPs. From the results of IR studies, specific bands for each compound (**PLGA** and **GNL**) were identified (Table 2). These specific vibrations were also observable for the nano-objects, highlighting the presence of both **PLGA** and **GNL** (Supporting Information Figure S1).

Due to the low proportion of **GNL** in the NPs, the band intensity was low. The  $\nu_{N=N}$  band was overlaid by other signals ( $\nu_{C=C}$ ), leading to the observation of a shoulder. Signal deconvolution using a Savitzky–Golay derivative was employed to separate signals from each pure compound (**PLGA** and **GNL**). Focusing on the **GNL** molecule and based on its first derivative spectrum, five specific signals (C=O, N=N, and C–O elongation vibrations, Table 2) were identified for **GNL**-loaded PLGA NPs. This result corroborates those obtained with the IR spectra and increased the number of signals related to the active compound. It confirms the presence of **GNL** in the PLGA NPs, even if at low concentration.

**Table 2.** Specific chemical bonds for PLGA, GNL, F1, and F3 in IR spectroscopy.

Chemical Bond (cm <sup>-1</sup> )	PLGA	GNL	F1	F3
O-H	3504.0	3388.3	3507.9	3507.9
C-H	2998.8–2883.1	2925.4/2854.1	2994.9–2854.1	2996.8–2854.1
C=O	1760.7	1702.8/1666.2/1637.3	1760.7	1760.7/1666.2/1639.2
N=N	N.A.	1537.0	N.A.	1535.1 (shoulder)
C=C	N.A.	1469.5	N.A.	N.A.
C-O	1454.1/1425.1/1396.2	1365.4–1047.2	1456.0/1425.1/1394.3	1454.1/1425.1/1394.3

### 3.3. GNL Quantification in PLGA Nanoparticles

Two quantification approaches were used to (i) quantify the free (or non-encapsulated) GNL and dATr and (ii) quantify the encapsulated GNL. The strategy for the free GNL was based on an enzymatic assay with UV quantification [39]. Indeed, the use of trehalase allowed the splitting of the trehalose into two glucose units which, after enzymatic reactions, enabled a detection at 340 nm. In the case of PLGA NP loaded with GNL or dATr, the concentrations of free active substances were found equivalent to zero, confirming their encapsulation and similar behavior (Supporting Information Figure S2). Regarding the DL and the drug EE, a destabilization of the nano-objects in basic conditions allowed the quantification of GNL by UV-Vis spectroscopy at 266.5 nm. A DL and an EE of 15% and 96%, respectively, were determined for F3 and agreed with the values usually found in the literature (Supporting Information Figure S3) [36].

### 3.4. Biocompatibility and Internalization of GNL Formulations

F2, F3, and F4 cytotoxicity at low concentration (1/1000°) was assessed in vitro on human neuroblastoma cell lines (i.e., BE(2)-M17 cells), given that previous studies showed that F1 and F5 were biocompatible at this concentration [19–22]. After an exposure of 24 h and 48 h, the tested formulations (F2, F3, and F4) did not exhibit significant toxicity compared to untreated cells (Figure 3A,B).

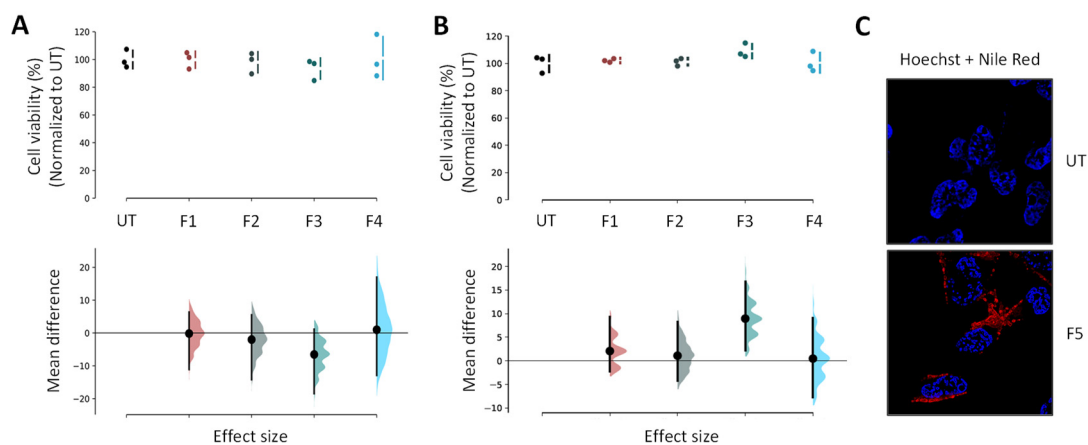


**Figure 3.** Biological evaluation of SLN and (un)loaded PLGA nanoparticles. (A) Cell viability evolution over time. BE(2)-M17 cells treated with F1 (red), F2 (dark blue), F3 (green), and F4 (cyan) compared to the untreated cells after (A) 24 h and (B) 48 h.  $n = 3$ .  $p < 0.05$  compared with untreated cells. (C) Representative images of F5 internalization in BE(2)-M17 cells after 24 h of exposure (1/1000°). Nuclei were stained with Hoechst (blue) and F5 was highlighted by the presence of Nile Red (red). Scale bar: 10 μm.

The next step corresponded to the evaluation of the cell internalization. As previously mentioned, a dedicated formulation containing Nile Red was prepared (F5) to evaluate cellular uptake. BE(2)-M17 cells (healthy neurons) were incubated in the presence of F5 diluted 1000 times for 24 h. As previously described [19–21], PLGA NPs were internalized

by cells (Figure 3C). Overall, the results obtained with the different formulations indicate their safety and cellular uptake at low concentration.

### 3.5. GNL-Loaded PLGA Nanoparticle Activity as Autophagy Inducer

The biological effects of the different formulations were further explored to monitor autophagic activity, following levels of the microtubule-associated protein, LC3, a key protein in the autophagy pathway, in the BE(2)-M17 healthy neuroblastoma cell line [30]. Trehalose-derivate nano-objects (F2, F3, F4, with the same concentration in trehalose) exhibited by immunoblot an accumulation of autophagosomes (APs) after exposure, compared with untreated cells, as indicated by increased levels in the AP marker LC3B-II in the cells (Figure 4A).

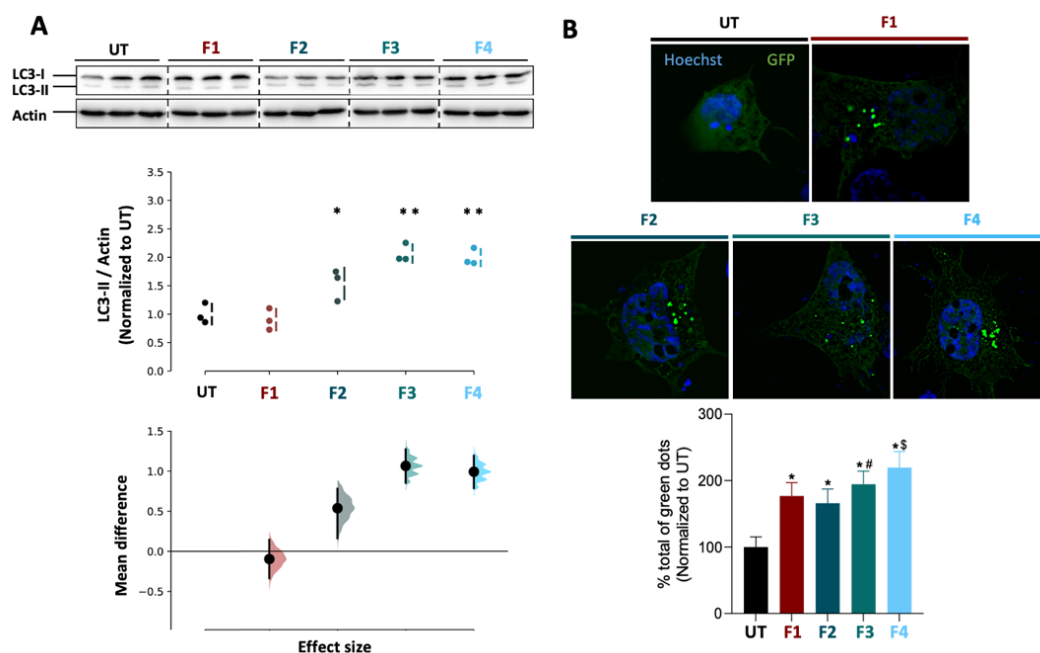


**Figure 4. Biological evaluation of SLN and (un)loaded PLGA nanoparticles.** (A) Immunoblot representative images and quantification of LC3 protein levels normalized by actin in BE (2)-M17 cells treated with F1 (red), F2 (dark blue), F3 (green) or F4 (cyan) for 24 h (1:1000).  $N = 3$ . \*  $p < 0.05$ , \*\*  $p < 0.005$  compared with untreated cells. (B) Quantification and images of LC3-positive dots per cell in BE (2)-M17 cells transfected with a GFP-LC3 plasmid for 24 h and treated with F1, F2, F3 or F4 for 24 h (1:1000). Scale bar: 10  $\mu\text{m}$ . \*  $p < 0.001$  compared with untreated cells; #  $p < 0.05$  compared with F2; \$  $p < 0.005$  compared with F2.  $n = 20$ .

In particular, F2 resulted in a 1.5-fold increase, while F3 and F4 significantly increased up to two-fold compared with UT conditions and molecular trehalose (used as control, Supporting Information Figure S4). These effects might be explained by the amphiphilic nature of NL and their resemblance to the lipid bilayer that composes cell membranes. NLs could cross the cell membrane more easily with or without the help of membrane transporters. These results indicate the beneficial effect of functionalizing the trehalose with a NL. The capacity to induce autophagy was further confirmed by immunofluorescence using a GFP-LC3 construct, which allowed the identification of AP-related vesicles. Further supporting an accumulation of AP in F2, F3 and F4-treated cells, GFP-positive vesicles were markedly increased in these treated cells, indicating an increase in AP numbers (Figure 4B). Of note, it is important to keep in mind in this immunofluorescence assay that we can underestimate the number of GFP-positive vesicles due to the dynamic turnover of GFP-LC3 in the autolysosome (i.e., the pH sensitivity of GFP) [40]. Taken together, these data indicate that GNL significantly modulated the autophagy in these cells.

#### 4. Conclusions

Herein, in order to develop new pharmaceutical nanotechnologies, the synthesis of a thymidine-derived GNL-bearing trehalose, as an active substance, to study their biocompatibility and ability to modulate autophagy for lysosomal impairment treatment was investigated. An amphiphilic molecule, named GNL, was designed and formulated into two different nanosystems, SLNs and PLGA NPs. These nano-objects were stable for at least 20 days at 4 °C and 10 days at 37 °C. The successful encapsulation of GNL inside PLGA NPs was confirmed by IR and UV-Visible spectroscopies (DL 15% and EE 96%). Cytotoxicity evaluation of GNL-loaded PLGA NPs and GNL-based SLN on human neuronal cells showed that GNLS are biocompatible at low concentration after 24 h of exposure. The uptake of fluorophore-loaded PLGA NPs into cells indicates that PLGA NPs are successfully internalized, highlighting the potential of these PLGA NPs as drug delivery systems. Moreover, immunoblotting and transfection assays suggest that GNL-based nanosystems improved biological activity of trehalose (two-fold) compared with molecular trehalose, thereby significantly modulating autophagy. These results suggest that GNL-based nanovectors can enhance the uptake of trehalose into cells and thus trehalose activity. Therefore, further *in vitro* studies will be carried out in a PD cellular model (M17 cells overexpressing  $\alpha$ -synuclein or BE(2)-M17 cells with depletion of lysosomal type 5 P-type ATPase (ATP13A2)) and further characterization, in particular autophagy flux experiments associated with GNL-based nanosystems will be assessed. GNL-loaded functionalized NPs will be developed and *in vivo* assays will be performed to evaluate their ability to cross the BBB and target neurons of interest, notably in order to modulate the pH and lysosomal activity.

**Supplementary Materials:** The following are available online at <https://www.mdpi.com/article/10.3390/pharmaceutics14040857/s1>, Figure S1: Infrared analysis of PLGA, GNL, and (un)loaded PLGA NPs; Figure S2: Principle of the enzymatic determination of trehalose; Figure S3: UV spectroscopy assays. Figure S4: Biological evaluation of trehalose.

**Author Contributions:** A.C., J.V., M.-L.T. and A.G. carried out experiments; P.B., L.L. and B.D. designed the experiments and revised the manuscript; A.C. analysed the data and wrote the manuscript; P.B. provided critical tool and reagents; P.B. and B.D. secured the funding. All authors have read and agreed to the published version of the manuscript.

**Funding:** The University of Bordeaux, and the Centre National de la Recherche Scientifique provided infrastructural support. This research was funded by *Le ministère de l'Enseignement supérieur, de la Recherche et de l'Innovation* (France) and by *Le collège des écoles doctorales (appel doctorat interdisciplinaire 2018)*. This study received financial support from the French government in the framework of the University of Bordeaux's IdEx "Investments for the Future" program/GPR BRAIN\_2030. This work was supported by grants from ANR-21-CE18-0025-01 NOVEL, Fondation de France (number 00066525) and an IDEX Emergence Grant number OPE-2018-410 (B.D.).

**Institutional Review Board Statement:** Not applicable.

**Informed Consent Statement:** Not applicable.

**Data Availability Statement:** The original contributions presented in the study are included in the article, further inquiries can be directed to the corresponding author.

**Acknowledgments:** We dedicate this article in memory of our research advisor, mentor, colleague and friend, Laurent Latxague. We thank Bordeaux Imaging Center (BIC) for technical support during TEM observations. We would like to thank J. Leblond Chain for her scientific advices.

**Conflicts of Interest:** The authors declare no conflict of interest.

#### References

1. Nichols, E.; Szeoke, C.E.I.; Vollset, S.E.; Abbasi, N.; Abd-Allah, F.; Abdela, J.; Aichour, M.T.E.; Akinyemi, R.O.; Alahdab, F.; Asgedom, S.W.; et al. Global, regional, and national burden of Alzheimer's disease and other dementias, 1990–2016: A systematic analysis for the Global Burden of Disease Study 2016. *Lancet Neurol.* **2019**, *18*, 88–106. [CrossRef]

2. Tysnes, O.-B.; Storstein, A. Epidemiology of Parkinson's disease. *J. Neural Transm.* **2017**, *124*, 901–905. [[CrossRef](#)] [[PubMed](#)]
3. Dehay, B.; Martinez-Vicente, M.; Caldwell, G.A.; Caldwell, K.A.; Yue, Z.; Cookson, M.R.; Klein, C.; Vila, M.; Bezd, E. Lysosomal impairment in Parkinson's disease. *Mov. Disord.* **2013**, *28*, 725–732. [[CrossRef](#)] [[PubMed](#)]
4. Emanuele, E. Can Trehalose Prevent Neurodegeneration? Insights from Experimental Studies. *Curr. Drug Targets* **2014**, *15*, 551–557. [[CrossRef](#)] [[PubMed](#)]
5. Korolenko, T.A.; Dubrovina, N.I.; Ovsyukova, M.V.; Bgatova, N.P.; Tenditnik, M.V.; Pupyshv, A.B.; Akopyan, A.A.; Goncharova, N.V.; Lin, C.L.; Zavjalov, E.L.; et al. Treatment with autophagy inducer trehalose alleviates memory and behavioral impairments and neuroinflammatory brain processes in db/db mice. *Cells* **2021**, *10*, 2557. [[CrossRef](#)] [[PubMed](#)]
6. Jeong, S.J.; Stitham, J.; Evans, T.D.; Zhang, X.; Rodriguez-Velez, A.; Yeh, Y.S.; Tao, J.; Takabatake, K.; Epelman, S.; Lodhi, I.J.; et al. Trehalose causes low-grade lysosomal stress to activate TFEB and the autophagy-lysosome biogenesis response. *Autophagy* **2021**, *17*, 3740–3752. [[CrossRef](#)]
7. Mancini, R.J.; Lee, J.; Maynard, H.D. Trehalose glycopolymers for stabilization of protein conjugates to environmental stressors. *J. Am. Chem. Soc.* **2012**, *134*, 8474–8479. [[CrossRef](#)]
8. Liu, R.; Barkhordarian, H.; Emadi, S.; Chan, B.P.; Sierks, M.R. Trehalose differentially inhibits aggregation and neurotoxicity of beta-amyloid 40 and 42. *Neurobiol. Dis.* **2005**, *20*, 74–81. [[CrossRef](#)]
9. Sarkar, S.; Davies, J.E.; Huang, Z.; Tunnacliffe, A.; Rubinsztein, D.C. Trehalose, a novel mTOR-independent autophagy enhancer, accelerates the clearance of mutant huntingtin and  $\alpha$ -synuclein. *J. Biol. Chem.* **2007**, *282*, 5641–5652. [[CrossRef](#)]
10. Khalifeh, M.; Barreto, G.E.; Sahebkar, A. Trehalose as a promising therapeutic candidate for the treatment of Parkinson's disease. *Br. J. Pharmacol.* **2019**, *176*, 1173–1189. [[CrossRef](#)]
11. Tanaka, M.; Machida, Y.; Niu, S.; Ikeda, T.; Jana, N.R.; Doi, H.; Kurosawa, M.; Nekooki, M.; Nukina, N. Trehalose alleviates polyglutamine-mediated pathology in a mouse model of Huntington disease. *Nat. Med.* **2004**, *10*, 148–154. [[CrossRef](#)] [[PubMed](#)]
12. Naqvi, S.; Panghal, A.; Flora, S.J.S. Nanotechnology: A Promising Approach for Delivery of Neuroprotective Drugs. *Front. Neurosci.* **2020**, *14*, 1–26. [[CrossRef](#)] [[PubMed](#)]
13. Teleanu, D.M.; Negut, I.; Grumezescu, V.; Grumezescu, A.M.; Teleanu, R.I. Nanomaterials for drug delivery to the central nervous system. *Nanomaterials* **2019**, *9*, 371. [[CrossRef](#)] [[PubMed](#)]
14. Cunha, A.; Gaubert, A.; Latxague, L.; Dehay, B. PLGA-Based Nanoparticles for Neuroprotective Drug Delivery in Neurodegenerative Diseases. *Pharmaceutics* **2021**, *13*, 1042. [[CrossRef](#)] [[PubMed](#)]
15. Essa, D.; Kondiah, P.P.D.; Choonara, Y.E.; Pillay, V. The Design of Poly(lactide-co-glycolide) Nanocarriers for Medical Applications. *Front. Bioeng. Biotechnol.* **2020**, *8*, 1–20. [[CrossRef](#)]
16. He, H.; Yao, J.; Zhang, Y.; Chen, Y.; Wang, K.; Lee, R.J.; Yu, B.; Zhang, X. Solid lipid nanoparticles as a drug delivery system to across the blood-brain barrier. *Biochem. Biophys. Res. Commun.* **2019**, *519*, 385–390. [[CrossRef](#)]
17. Benizri, S.; Ferey, L.; Alies, B.; Mebarek, N.; Vacher, G.; Appavoo, A.; Staedel, C.; Gaudin, K.; Barthélémy, P. Nucleoside-Lipid-Based Nanocarriers for Sorafenib Delivery. *Nanoscale Res. Lett.* **2018**, *13*, 17. [[CrossRef](#)]
18. Makadia, H.K.; Siegel, S.J. Poly Lactic-co-Glycolic Acid (PLGA) as biodegradable controlled drug delivery carrier. *Polymers* **2011**, *3*, 1377–1397. [[CrossRef](#)]
19. Bourdenx, M.; Daniel, J.; Genin, E.; Soria, F.N.; Blanchard-Desce, M.; Bezd, E.; Dehay, B. Nanoparticles restore lysosomal acidification defects: Implications for Parkinson and other lysosomal-related diseases. *Autophagy* **2016**, *12*, 472–483. [[CrossRef](#)]
20. Zeng, J.; Martin, A.; Han, X.; Shirihi, O.S.; Grinstaff, M.W. Biodegradable plga nanoparticles restore lysosomal acidity and protect neural pc-12 cells against mitochondrial toxicity. *Ind. Eng. Res.* **2019**, *58*, 13910–13917. [[CrossRef](#)]
21. Prévot, G.; Soria, F.N.; Thiolat, M.L.; Daniel, J.; Verlhac, J.B.; Blanchard-Desce, M.; Bezd, E.; Barthélémy, P.; Crauste-Manciet, S.; Dehay, B. Harnessing Lysosomal pH through PLGA Nanoemulsion as a Treatment of Lysosomal-Related Neurodegenerative Diseases. *Bioconjug. Chem.* **2018**, *29*, 4083–4089. [[CrossRef](#)] [[PubMed](#)]
22. Arotcarena, M.L.; Soria, F.N.; Cunha, A.; Doudnikoff, E.; Prévot, G.; Daniel, J.; Blanchard-Desce, M.; Barthélémy, P.; Bezd, E.; Crauste-Manciet, S.; et al. Acidic nanoparticles protect against  $\alpha$ -synuclein-induced neurodegeneration through the restoration of lysosomal function. *Aging Cell* **2022**, *23*, e13584. [[CrossRef](#)] [[PubMed](#)]
23. Simeone, L.; Milano, D.; De Napoli, L.; Irace, C.; Di Pascale, A.; Boccalon, M.; Tecilla, P.; Montesarchio, D. Design, Synthesis and Characterisation of Guanosine-Based Amphiphiles. *Chem. Eur. J.* **2011**, *17*, 13854–13865. [[CrossRef](#)] [[PubMed](#)]
24. Hynie, S.; Smrt, J. Effects of adenosine 5'-phosphate esters with lipid hydroxy compounds (adenosine nucleolipids) on the activity of enzymes of cyclic AMP system. *FEBS Lett.* **1978**, *94*, 339–341. [[CrossRef](#)]
25. Van Tiel, F.H.; Boere, W.A.M.; Harmsen, T.; Kraaijeveld, C.A.; Snippe, H. Determination of inhibitory concentrations of antiviral agents in cell culture by use of an enzyme immunoassay with virus-specific, peroxidase-labeled monoclonal antibodies. *Antimicrob. Agents Chemother.* **1985**, *27*, 802–805. [[CrossRef](#)]
26. Chabaud, P.; Camplo, M.; Payet, D.; Serin, G.; Moreau, L.; Barthélémy, P.; Grinstaff, M.W. Cationic nucleoside lipids for gene delivery. *Bioconjug. Chem.* **2006**, *17*, 466–472. [[CrossRef](#)]
27. Scheidt, H.A.; Flasche, W.; Cismas, C.; Rost, M.; Herrmann, A.; Liebscher, J.; Huster, D. Design and application of lipophilic nucleosides as building blocks to obtain highly functional biological surfaces. *J. Phys. Chem. B* **2004**, *108*, 16279–16287. [[CrossRef](#)]
28. Allain, V.; Bourgaux, C.; Couvreur, P. Self-assembled nucleolipids: From supramolecular structure to soft nucleic acid and drug delivery devices. *Nucleic Acids Res.* **2012**, *40*, 1891. [[CrossRef](#)]

29. Swastika; Chaturvedi, S.; Kaul, A.; Hazari, P.P.; Jha, P.; Pal, S.; Lal, S.; Singh, B.; Barthélémy, P.; Mishra, A.K. Evaluation of BBB permeable nucleolipid (NLDPU): A di-C15-ketalised palmitone appended uridine as neuro-tracer for SPECT. *Int. J. Pharm.* **2019**, *565*, 269–282. [[CrossRef](#)]
30. Colombo, E.; Biocotino, M.; Frapporti, G.; Randazzo, P.; Christodoulou, M.S.; Piccoli, G.; Polito, L.; Seneci, P.; Passarella, D. Nanolipid-Trehalose Conjugates and Nano-Assemblies as Putative Autophagy Inducers. *Pharmaceutics* **2019**, *11*, 422. [[CrossRef](#)]
31. Mandal, S.; Debnath, K.; Jana, N.R.; Jana, N.R. Trehalose-Functionalized Gold Nanoparticle for Inhibiting Intracellular Protein Aggregation. *Langmuir* **2017**, *33*, 13996–14003. [[CrossRef](#)] [[PubMed](#)]
32. Debnath, K.; Pradhan, N.; Singh, B.K.; Jana, N.R.; Jana, N.R. Poly(trehalose) Nanoparticles Prevent Amyloid Aggregation and Suppress Polyglutamine Aggregation in a Huntington’s Disease Model Mouse. *ACS Appl. Mater. Interfaces* **2017**, *9*, 24126–24139. [[CrossRef](#)] [[PubMed](#)]
33. Betancourt, T.; Brown, B.; Brannon-Peppas, L. Doxorubicin-loaded PLGA nanoparticles by nanoprecipitation: Preparation, characterization and in vitro evaluation. *Nanomedicine* **2007**, *2*, 219–232. [[CrossRef](#)] [[PubMed](#)]
34. Huang, W.; Zhang, C. Tuning the Size of Poly(lactic-co-glycolic Acid) (PLGA) Nanoparticles Fabricated by Nanoprecipitation. *Biotechnol. J.* **2018**, *13*, 1700203. [[CrossRef](#)] [[PubMed](#)]
35. Rowan, A.S.; Nicely, N.I.; Cochrane, N.; Wlassoff, W.A.; Claiborne, A.; Hamilton, C.J. Nucleoside triphosphate mimicry: A sugar triazolyl nucleoside as an ATP-competitive inhibitor of *B. anthracis* pantothenate kinase. *Org. Biomol. Chem.* **2009**, *7*, 4029–4036. [[CrossRef](#)] [[PubMed](#)]
36. Evers, M.J.W.; Kulkarni, J.A.; van der Meel, R.; Cullis, P.R.; Vader, P.; Schiffelers, R.M. State-of-the-Art Design and Rapid-Mixing Production Techniques of Lipid Nanoparticles for Nucleic Acid Delivery. *Small Methods* **2018**, *2*, 1700375. [[CrossRef](#)]
37. Moghimi, S.M.; Hunter, A.C.; Murray, J.C. Long-circulating and target-specific nanoparticles: Theory to practice. *Pharmacol. Rev.* **2001**, *53*, 283–318.
38. Hoshyar, N.; Gray, S.; Han, H.; Bao, G. The effect of nanoparticle size on in vivo pharmacokinetics and cellular interaction. *Nanomedicine* **2016**, *11*, 673–692. [[CrossRef](#)]
39. Castillo, K.; Valenzuela, V.; Oñate, M.; Hetz, C. A Molecular Reporter for Monitoring Autophagic Flux in Nervous System In Vivo. *Methods Enzymol.* **2017**, *588*, 109–131. [[CrossRef](#)]
40. Ni, H.M.; Bockus, A.; Wozniak, A.L.; Jones, K.; Weinman, S.; Yin, X.M.; Ding, W.X. Dissecting the dynamic turnover of GFP-LC3 in the autolysosome. *Autophagy* **2011**, *7*, 188–204. [[CrossRef](#)]